

An Emerging Nanozyme Class for à la carte Enzymatic-Like Activities based on Protein-Metal Nanocluster Hybrids

Rocío López-Domene, Silvia Vázquez-Díaz, Evgenii Modin, Ana Beloqui,*
and Aitziber L. Cortajarena*

In this study, the goal is to fabricate robust and highly efficient peroxidase-like nanozymes that can ultimately be assembled into films for their easy reuse in catalytic cycles. Nanozymes are designed by mimicking the strategy adopted by metalloproteins to accommodate metal cofactors within their protein structure. The engineered consensus tetratricopeptide repeat (CTPR) protein module is selected as the scaffold to guide the growth and the stabilization of a library of in situ synthesized metal nanoclusters. A deep investigation of the interplay between the composition and function of the nanozymes reveals the impact of the protein templates and nanocluster composition on the peroxidase-like activity of the hybrids. Moreover, among a total of 24 hybrids, a top-performing nanozyme results from the growth of Au/Pt bimetallic nanoclusters on a CTPR protein with engineered histidine coordination sites. These nanozymes exhibit improved thermostability and resistance to hydrogen peroxide compared to natural peroxidases like horseradish peroxidase. Finally, it shows the easy fabrication of nanozyme composite films guided throughout the intrinsic self-assembling properties of the CTPR scaffold. These heterogeneous solid materials are reused in several reaction cycles without significant loss of the catalytic performance, proving these protein-templated nanozymes as an advantageous alternative to natural enzymes.

to overcome some of the limitations of natural biocatalysts.^[3,4] However, such an ambitious goal could only be achieved if the synthesized nanozymes exhibit both high catalytic performance and relevant robustness under broad operational conditions.^[3,5-7] While most of the developed nanozymes consist of inorganic nanoparticles (NPs), the use of ultra-small size NPs (≤ 2 nm) as potential nanozymes has not been exploited yet.^[8-10] These types of nanomaterials, composed of several to hundred metal atoms, are known as metal nanoclusters (mNCs).^[11,12] Among their numerous traits, mNCs are attractive due to their excellent catalytic profile, which generally overperforms that shown by inorganic NPs.^[13] Unfortunately, as they are susceptible to agglomeration into larger NPs, the synthesis of high-quality mNCs is still challenging.^[14] Only the template-guided growth of mNCs has been successfully demonstrated to achieve controlled reduction of cationic sources and avoid the formation of undesired aggregates.^[11,15,16] The selection of the appropriate template is key to modulate the final features


of the mNCs and enable the implementation of the nanozymes in specific fields. Therefore, the use of engineered small ligands,^[17] metal organic frameworks,^[18] or biomacromolecules such as antibodies^[19] permits the application of mNCs as bioimaging agents, photocatalysts, or sensing probes, respectively.

1. Introduction

Nanozymes are (in)organic materials featured as artificial biocatalysts due to their small dimensions and excellent catalytic performance in several chemical reactions.^[1,2] These emerging nanomaterials have been proposed as artificial alternatives

R. López-Domene, S. Vázquez-Díaz, A. L. Cortajarena
Center for Cooperative Research in Biomaterials (CIC biomaGUNE)
Basque Research and Technology Alliance (BRTA)
Paseo de Miramón 194, Donostia-San Sebastián 20014, Spain
E-mail: alcortajarena@cicbiomagune.es

R. López-Domene, A. Beloqui
POLYMAT and Department of Applied Chemistry
Faculty of Chemistry
University of the Basque Country UPV/EHU
Paseo Manuel Lardizabal 3, Donostia-San Sebastián 20018, Spain
E-mail: ana.beloqui@ehu.es

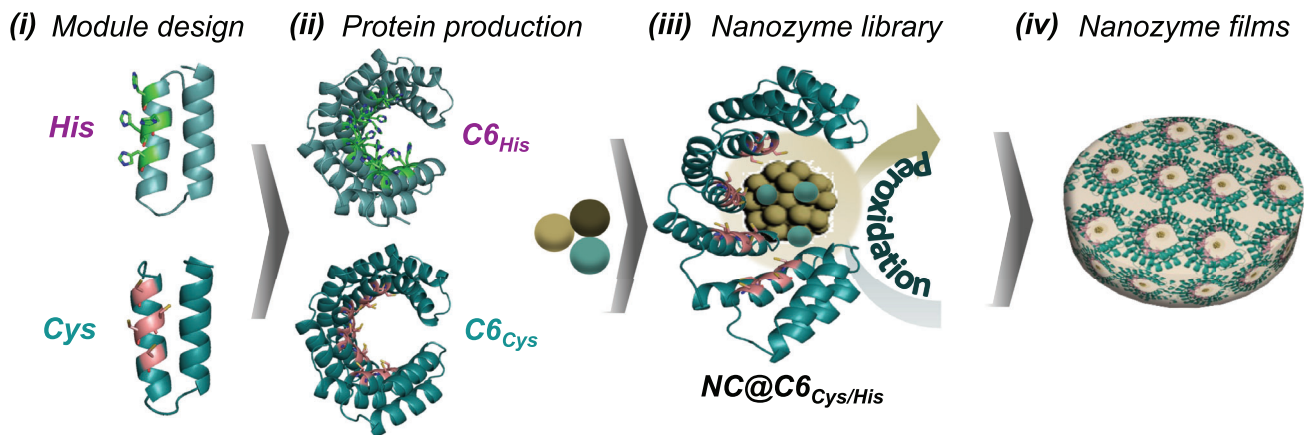
 The ORCID identification number(s) for the author(s) of this article can be found under <https://doi.org/10.1002/adfm.202301131>

E. Modin
Center for Cooperative Research in Nanomaterials (CIC nanoGUNE)
Basque Research and Technology Alliance (BRTA)
Avenida Tolosa 14, Donostia-San Sebastián 20018, Spain

© 2023 The Authors. Advanced Functional Materials published by Wiley-VCH GmbH. This is an open access article under the terms of the Creative Commons Attribution License, which permits use, distribution and reproduction in any medium, provided the original work is properly cited.

A. Beloqui, A. L. Cortajarena
IKERBASQUE
Basque Foundation for Science
Plaza Euskadi 5, Bilbao 48009, Spain

DOI: 10.1002/adfm.202301131



Scheme 1. Proposed experimental workflow for the fabrication of nanozyme films with peroxidase-like activity. Engineered CTPR motifs with 4 metal-coordinating histidines or cysteines at the positions 2, 6, 9, and 13 of the 34 amino acid CTPR sequence are designed (i). Engineered modules are combined and flanked with unmodified WT CTPR modules to give rise to the final constructs with 6 repeated domains and 16 metal coordinating amino acids that are conveniently allocated on the concave face of the proteins. Proposed structures for $C6_{His}$ and $C6_{Cys}$ are shown based on CTPR-WT structure (PDB DI: 2AVP). (ii). Metal nanoclusters are grown in the inner cavity of the protein, as depicted in the proposed structure, upon the addition of corresponding metal salts and the subsequent in situ reduction. Hence, a library of nanozymes is produced, characterized, and their peroxidase-like activity tested (iii). Finally, the top-performing nanozyme is used to fabricate solid catalytic films (iv).

Inspired by nature, specifically by the configuration and composition of metalloproteins, metal-loaded protein scaffolds have emerged. As for metalloenzymes, optimized coordination environments are offered to specific metal cofactors, either metal clusters or single metal ions.^[20–23] The use of proteins as scaffolds to accommodate metal catalysts has been promoted as a green strategy for the synthesis of biocompatible and easy-to-handle catalytic biomaterials.^[16,24,25] Such bio-scaffolds are often manipulated to accommodate artificially inserted metal cofactors through metal substitution or metal coordination pathways.^[26] Metal NCs have also been accommodated within commercially available protein templates such as BSA, lysozyme, and ferritin.^[27–29] Yet, the use of protein templates that lack armored metal-binding sites usually leads to the uncontrolled formation of NPs and aggregates, limiting their usefulness in catalytic processes.^[30] Therefore, alternative strategies based on the molecular engineering of the protein scaffold to ultimately stabilize the mNCs are sought. In this regard, we hypothesize the integration of the new native metal-binding sites into natural scaffolds without any preexisting metal coordination is an attractive approach for the fine-tuned localization and the stabilization of mNCs. Hence, powerful protein-templated mNCs with controlled environment and composition could be achieved.^[31,32] While the bio-scaffold would impart colloidal stability to the inorganic counterpart, precluding the formation of aggregates and controlling the synthesis procedure, the catalytic robustness of the hybrid would be governed by the catalytic capabilities of the mNCs, which are less delicate to conformational changes than metalloenzymes. The role of the protein scaffold on the stability and catalytic performance of the nanozymes is explored in this study.

Endorsed by the current technological and industrial applications, catalysts recovery after the catalytic reaction is an essential requirement for their reusability.^[33] There are several methodologies for the embedment of enzymes on solid supports,^[34–39] but

only limited approximations to integrate nanozymes, and more specifically mNCs, on solid materials have been reported.^[32] In this regard, we present the selection of structural proteins with the ability to self-assemble into manipulable films as an excellent opportunity to achieve tunable mNCs-loaded heterogeneous nanozymes that enable the reuse of the catalytic material in multiple consecutive reactions.^[40,41]

In this work, designed repeat proteins, namely consensus tetratricopeptide repeat proteins (CTPR), were chosen due to their exceptional modular features.^[31,32,42–45] The 3D structure of CTPR is defined by few conserved residues (9 out of 34), which enables the tailoring of the protein sequence without exerting conformational alterations. Here, CTPR proteins with six repeats and engineered metal coordination sites encoded by cysteines ($C6_{Cys}$) or histidines ($C6_{His}$) were envisaged as optimized environments for the growth of mNCs, which were synthesized following green chemistry premises in a one-pot synthesis procedure.^[31] Hence, a library of novel nanozymes that mimic the structure of metalloproteins with peroxidase-like activity was attempted (Scheme 1). Interesting results are revealed when compared to a natural peroxidase enzyme, the horseradish peroxidase (HRP). To conclude, we explored the capability to self-assemble these hybrid nanozymes into robust solid films for reusability purposes.

2. Results and Discussion

2.1. Synthesis and Characterization of Monometallic Nanozymes

Herein selected protein scaffold, the consensus tetratricopeptide repeats (CTPR) protein, was engineered to introduce metal-coordinating sites based on histidine or cysteine sequences that are strategically allocated and oriented to accommodate metal cations.^[32,46,47] Optimized scaffolds were designed with six CTPR modules composed of four engineered repeats with 4 histidines or 4 cysteines per module and two wild-type (WT) flanking

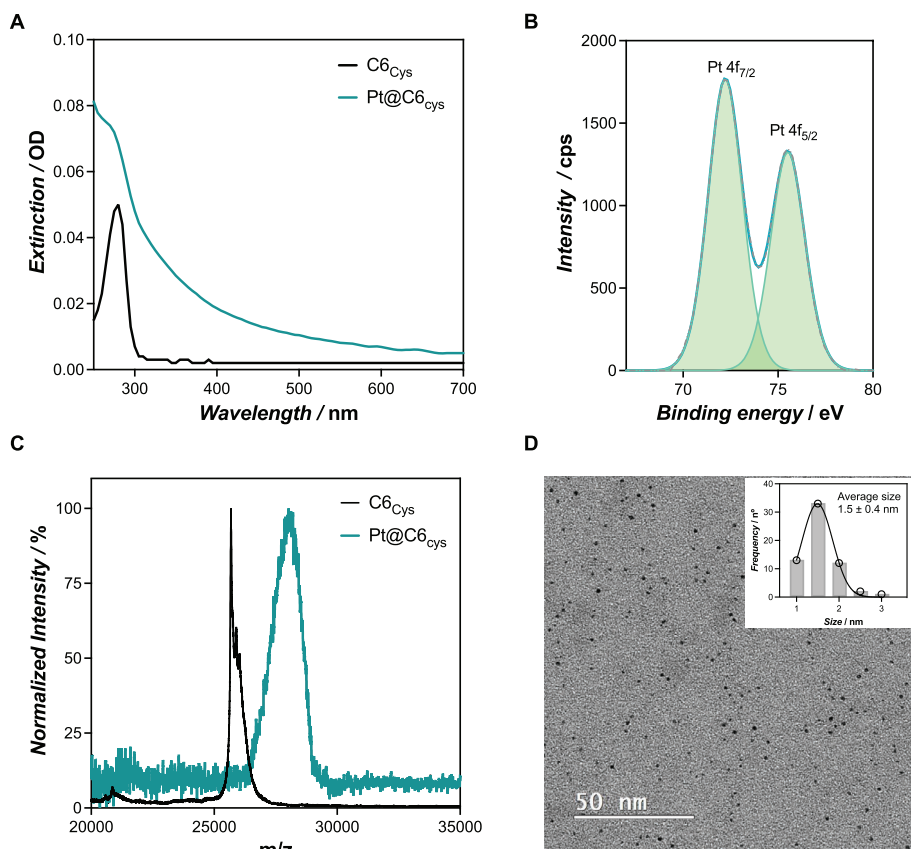


Figure 1. Characterization of Pt@C6_{Cys} nanozyme. A) UV-vis spectra of the protein scaffold with (in green) and without (in black) the nanocluster. B) Deconvolution analysis of high-resolution XPS spectrum of the Pt 4f peaks measured for Pt@C6_{Cys}. C) MALDI-ToF spectra of the CTPR protein (m/z of 25 738) and Pt@C6_{Cys} (m/z of ca. 28 000). D) TEM image of the Pt@C6_{Cys} sample. The inset image shows the size distribution of the Pt nanozymes.

repeats. These configurations resulted in protein scaffolds with a total of 16 histidine or cysteine residues and are here referred to as C6_{His} and C6_{Cys} variants, respectively (Scheme 1i,ii). The distribution of these residues was determined based on the following design principles: i) the residues should point toward the inner cavity of the protein to generate a protective environment for the accommodation of the nanoclusters; ii) selected residues should be exposed to the environment to allow the metal-ligand coordination; iii) non-conserved residues were chosen based on previous analysis of sequence conservation within TPR domains,^[48] which can be modified while guaranteeing the preservation of the TPR fold; and iv) previous observations indicated that increasing the number of coordinating residues per repeat to four could increase the size of the resulting metallic nanoclusters.^[46] Further details on the protein design, expression, and purification are described in the Experimental Section.

The synthesis of the mNCs was performed using the engineered CTPR variants as templates to achieve gold, copper, or platinum nanocluster-loaded nanozymes, referred to as mNCs@C6, in a procedure that avoids the use of organic solvents and stabilizing agents. It is worth noting that the protein structure is not preserved throughout the complete synthesis procedure, and thus it may function as a carrier of high local concentration of coordinating His or Cys residues at this stage. However, the robustness of the CTPR structure enables correct refold-

ing to occur upon the synthesis, proving a structured environment to the final nanoclusters (Figure S1, Supporting Information). The synthesis protocol entails the incubation of the engineered proteins and corresponding metal salts (HAuCl₄, CuSO₄, or K₂PtCl₄), and the in situ reduction of the inorganic components using sodium ascorbate as reducing agent (Scheme 1iii). Thereafter, samples were washed and purified according to the protocol described in the Experimental Section. The composition of the yielded hybrids was enlightened by several spectroscopic techniques. UV-vis spectra of the nanozymes profiled the contribution of the protein absorption at 280 nm together with an increase in the extinction in the visible range of the spectra corresponding to the mNCs (Figure 1A; Figure S2, Supporting Information). Circular dichroism spectroscopy on mNCs@C6 did not provide clear results due to the absorption and scattering imparted by the nanoclusters. However, the signature signal of the α -helical content was appreciated, indicating that the protein scaffold presumably conserved the characteristic α -helical secondary structure upon the synthesis procedure (Figure S3, Supporting Information), as previously reported for CTPR-stabilized mNCs.^[46] The presence of inorganic components and their corresponding oxidation states were examined by X-Ray Photoelectron Spectroscopy (XPS). Under these synthesis conditions, we achieved Pt-based nanozymes composed exclusively by oxidized species, namely Pt^{II} (Figure 1B). Contrarily, the

synthesis procedure led to a nearly complete reduction of copper and gold salts (Figure S4, Supporting Information). As for Cu@C6_{His}, two distinct peaks at 930.7 and 950.4 eV were assigned to Cu 2p_{3/2} and Cu 2p_{1/2} with a spin-orbit separation of 19.7 eV, respectively. These peaks confirmed the presence of Cu⁰ and only trace amounts of Cu^I.^[49] Similar information was retrieved from Au@C6, in which Au⁰ could only be observed as the main specie.

A precise analysis of the atomic size of the mNCs was performed by Inductively Coupled Plasma Mass Spectrometry (ICP-MS) (Table 1; and Table S1, Supporting Information). Interestingly, the number of metal atoms coordinated per protein and, thereby, the size of the mNCs, relied not only on the type and concentration of the offered metal cation but also on the composition of the engineered scaffold. As a general trend, C6_{Cys} was able to accommodate metal cations with higher efficiency than C6_{His}. Furthermore, our methodology fosters the growth of Pt NCs over Au or Cu NCs regardless of the coordination sphere in which the nanoclusters are settled, with more than 20 Pt atoms per protein tracked by ICP-MS for Pt@C6_{Cys/His} nanozymes. We confirmed the complete modification of the recovered protein by Matrix-Assisted Laser Desorption/Ionization Time-of-Flight mass spectrometry (MALDI-ToF) (Figure 1C; Figure S5 and Table S2, Supporting Information), since no unmodified protein was detected after the synthesis procedure. The yield of the process, measured as the % of the recovered protein, varied from 22 to 80%, and depended on the metal source and the protein scaffold used for the synthesis (Table S3, Supporting Information). Finally, a size of 1.5 ± 0.4 nm was determined for Pt nanozymes by Transmission Electron Microscopy (TEM) (Figure 1D).

The catalytic performance of the newly prepared hybrids was characterized. The peroxidation capability of the nanozymes was followed by monitoring the oxidation of pyrogallol (PG) to purpurogallin in presence of hydrogen peroxide at 420 nm (Figure S6 and Table S4, Supporting Information). As shown in Table 1, no significant differences in terms of catalytic turnovers were observed for a given mNC when comparing the two protein scaffolds. However, relevant differences arose from the nature of the metal component of the nanozyme. Pt@C6 exhibited the highest catalytic turnovers, performing almost 50 times faster than Cu@C6 hybrids. In addition, we demonstrated that the protein template provided significant benefit for the stabilization and cat-

alytic performance of Pt and Cu nanoclusters compared to naked nanoclusters (Figure S7, Supporting Information). Yet, Au@C6 was not able to oxidize PG under identical conditions.

2.2. Expanding the Catalytic Scope of the Hybrid Nanozymes

Although this optimized protocol was successful for the fabrication of catalytically active nanozymes, we observed that monometallic hybrids showed limited growth of the inorganic components. Moreover, we could not achieve the reduction of Pt atoms in situ following our protocol. Thereby, supported by previous reports,^[50,51] we envisioned that the formulation of nanozymes with bimetallic nanoclusters (bmNC@C6) could outperform the catalytic activity measured for mNCs. Consequently, we attempted to experimentally evolve the inorganic component of the hybrids by triggering the in situ assembly of bmNCs on the engineered metal coordination proteins (both His- and Cys-based). Starting from the top-performing sample, i.e., Pt@C6, we achieved Pt hybrids doped with either Au or Cu atoms at a range of molar dilutions (Au/Cu:Pt molar ratios of 1:2, 1:6, and 1:10). To understand the system further, a nanozyme family composed by Au and Cu was also built (Table 2). The same synthesis conditions were applied to both C6_{His} and C6_{Cys} variants to assess the effect of the engineered modules on the growth of bmNCs. Hence, we achieved a library of 18 bimetallic nanozymes that was fully characterized in terms of their chemical composition, catalytic performance, and stability, in order to be considered as valuable replacements of natural enzymes for selected applications (details on the synthesis in the Experimental Section). Nanozymes were coded according to their metal composition with the M1_xM2_y@C6_{His/Cys} nomenclature, where M1 and M2 refer to the metal components of the NC (Au, Cu, or Pt) and *x* and *y* indicate the number of atoms present within the nanozyme, as revealed by ICP-MS (Table 2; and Table S5, Supporting Information).

At first glance, larger clusters were obtained when higher metal concentrations were offered to the protein. Moreover, it seems that the incorporation of Pt constrains the overall insertion of Au and Cu atoms within the NCs. A clear example of this effect can be found when using C6_{His} as scaffold. For the same Au concentration, the addition of 5 times more of Pt salt restricted the incorporation of Au from 14 to 7 atoms within the nanozyme (reaction 4a vs 6a in Table 2, respectively). Another interesting trend denoted that the Au_xPt_y formulation yielded larger clusters than Cu_xPt_y, with only 2 to 3 atoms of Cu incorporated in the Cu_xPt_y series. At this point, unlike shown by mNCs, the binding module also exerted a clear difference. Under the same reaction conditions, 6a and 6b in Table 2, the use of the Cys scaffold gave rise to larger nanoclusters, with 30% higher atom content — with an incorporation of 83 versus 57 total atoms using C6_{Cys} or C6_{His} modules, respectively. Contrarily, when Cu_xPt_y clusters were examined under the same reaction conditions (9a and 9b in Table 2), larger structures were achieved when using the C6_{His} template compared to C6_{Cys} (41 vs 30 total atoms, respectively). It is known that gold binds most efficiently to thiols within cysteines,^[52–54] and that copper preferentially is coordinated by the imidazole rings within histidines,^[55] thus the strength in the coordination of the nucleating metal might determine the final size of the

Table 1. Characterization of monometallic mNCs@C6. ICP-MS (as number of atoms per protein) and peroxidase-like activity (^{app}k_{cat}, s⁻¹) results for Au, Cu, and Pt monometallic NCs stabilized by C6_{His} and C6_{Cys} proteins.

No. Reaction	Offered metal equivalents ^{a)}	Template	Final composition ^{b)}	Peroxidase-like activity [^{app} k _{cat} , s ⁻¹]
1a	64 (Au)	C6 _{His}	Au ₅	–
1b		C6 _{Cys}	Au ₈	–
2a	64 (Cu)	C6 _{His}	Cu ₅	36.4 ± 1.0
2b		C6 _{Cys}	Cu ₁₁	31.6 ± 1.6
3a	64 (Pt)	C6 _{His}	Pt ₂₀	1487.8 ± 97.7
3b		C6 _{Cys}	Pt ₂₄	1512.3 ± 24.7

^{a)} Equivalents with respect to the protein. ^{b)} As measured by ICP-MS.

Table 2. Synthesis conditions utilized for the fabrication of bimetallic NCs of Au_xPt_y, Au_xCu_y, and Cu_xPt_y and the measurement of the final atomic composition of the clusters.

No. Reaction	Offered metal concentration [mM]	Offered Au equivalents ^{a)}	Offered Pt equivalents ^{a)}	Offered Cu equivalents ^{a)}	Template	Final composition ^{b)}
4a	1.92	32	64	-	C6 _{His}	Au ₁₄ Pt ₁₂
4b					C6 _{Cys}	Au ₉ Pt ₈
5a	4.48	32	192	-	C6 _{His}	Au ₁₀ Pt ₄₂
5b					C6 _{Cys}	Au ₅ Pt ₅₇
6a	7.04	32	320	-	C6 _{His}	Au ₇ Pt ₅₀
6b					C6 _{Cys}	Au ₇ Pt ₇₆
7a	1.92	-	64	32	C6 _{His}	Cu ₂ Pt ₈
7b					C6 _{Cys}	Cu ₂ Pt ₅
8a	4.48	-	192	32	C6 _{His}	Cu ₃ Pt ₂₇
8b					C6 _{Cys}	Cu ₂ Pt ₁₅
9a	7.04	-	320	32	C6 _{His}	Cu ₂ Pt ₃₉
9b					C6 _{Cys}	Cu ₃ Pt ₂₇
10a	1.92	32	-	64	C6 _{His}	Au ₁₄ Cu ₃
10b					C6 _{Cys}	Au ₁₈ Cu ₃
11a	4.48	32	-	192	C6 _{His}	Au ₁₂ Cu ₂₀
11b					C6 _{Cys}	Au ₇ Cu ₇
12a	7.04	32	-	320	C6 _{His}	Au ₁₇ Cu ₁₂
12b					C6 _{Cys}	Au ₇ Cu ₁₂

^{a)} Equivalents with respect to the protein. ^{b)} As measured by ICP-MS.

bmNC. From the whole library, Au₇Pt₇₆@C6_{Cys} nanozyme was found to be the largest in terms of the number of atoms. A TEM image of this nanozyme revealed the formation of homogeneous nanoclusters with an average size of 2.3 ± 0.8 nm (Figure S8, Supporting Information).

To complete the compositional characterization of the nanozymes, we analyzed the oxidation states of the newly synthesized hybrids by XPS. Remarkably, unlike observed for monometallic NCs, bimetallic C6 hybrids displayed intermediate oxidation states such as Au^I, Au^{III}, and Cu^I (Figures S9–S11 and Table S6, Supporting Information). And more interestingly, reduced Pt⁰ species were now achieved, which are of high interest for catalysis (Figure 2A).^[56,57] As the size of the bmNCs increases, reduced species, namely Pt⁰, prevail for a given protein scaffold, as expected from larger nanocluster cores (Figure 2B).^[58,59] Interestingly, significant differences in the predominance of the oxidation states of the bmNCs are observed when either C6_{Cys} or C6_{His} scaffolds are used. For example, the higher reducing potential of the cysteines is observed for Cu_xPt_y@ nanozymes, as C6_{Cys} module triggers the reduction of platinum to Pt⁰ with more efficiency than C6_{His} (Figure 2C; Figure S10, and Table S6, Supporting Information).

2.3. Assessment of the Catalytic Performance of the Hybrids

2.3.1. Measurement of the Catalytic Parameters

The tunability of the oxidation states by the bmNC size, metal composition, and protein scaffold enables a rich protein-bmNC library that encompasses diverse redox properties of relevance

to catalysis. Therefore, the catalytic potential of this collection of nanozymes was explored. We detected that the nanozymes, relying upon their composition, exhibited peroxidase, oxidase, catalase, and superoxide dismutase-like activities (Figure S12, Supporting Information). In this work, we have focused our efforts on the assessment of the most prominent catalysis, namely, the peroxidation of the evolved bmNCs@C6 in relation to the catalytic profile of natural peroxidase, namely, horseradish peroxidase (HRP). For that, we performed a comprehensive study in which composition-function relationships were revealed through the correlation of the measured kinetic parameters and the unveiled composition of the hybrids.

bmNCs@C6 were considered artificial metalloenzymes as they displayed Michaelis-Menten-like kinetics.^[60] The measurements performed and the calculations of the apparent kinetic parameters ($^{app}K_M$, $^{app}V_{max}$, $^{app}k_{cat}$, and $^{app}k_{cat}/^{app}K_M$) for the peroxidation of pyrogallol (PG) are collected in Figures S13–S15 and Table S7 (Supporting Information). All the bimetallic biohybrids showed peroxidase-like activity to a greater or lesser extent. As expected, hybrids with Pt in their formulation provided better catalytic performances than Au_xCu_y series (Figure 3A). Moreover, the bmNCs within the Au_xCu_y family of nanozymes outperformed monometallic Cu@C6 hybrids, in agreement with previous works that reported on the enhanced activity of bi-metallic systems (Figure 3A, inset figures).^[61,62] Further, the $^{app}k_{cat}$ of Au_xPt_y@C6_{Cys} series did not evolve significantly with the size of the NCs as observed for the Au_xPt_y@C6_{His} nanozymes. Largest NCs rendered $^{app}k_{cat}$ values of 3667 s⁻¹, only 2.4 times higher than the value measured for the monometallic Pt@C6_{Cys}. This effect might be related to the orientation of the growth of the clusters on the Cys module, which might exert diffusion limitations to

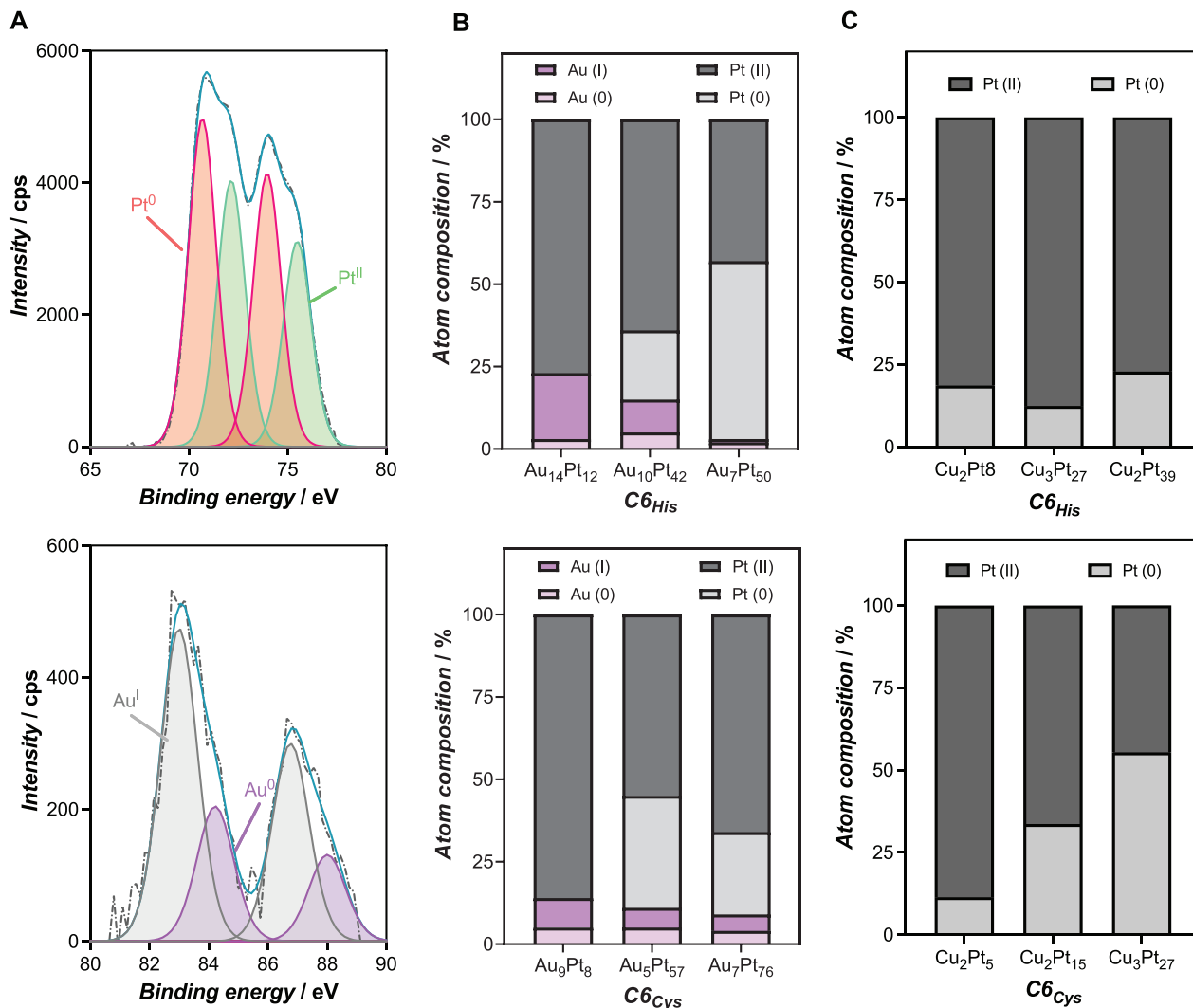


Figure 2. Deconvolution analysis of high-resolution XPS spectra of the Cu 2p, Au 4f, and Pt 4f peaks measured for Au_xPt_y@ and Cu_xPt_y@ nanozymes. A) Fitting curves of Pt 4f_{7/2} spectra (up) and Au 4f_{5/2} (down) of Au₅Pt₅₇@C_{6His} hybrid. B,C) Atom composition (as %) and their corresponding oxidation states for Au_xPt_y@ (B) and Cu_xPt_y@ (C) nanozymes. The traces of Cu could not be detected by XPS.

the catalytic event. Contrarily, C_{6His} module allowed a significant evolution of the performance of the NCs in terms of the catalytic turnover, showing a maximum of 12 640 s⁻¹, which results in 8.5 times the value measured for the monometallic Pt@C_{6His} and in 3.4 times the best result obtained for the C_{6Cys} variants, i.e., Au₇Pt₇₆@C_{6Cys}.

Both modules, i.e., C_{6His} and C_{6Cys}, showed an overall correlation between the number of Pt atoms incorporated into the cluster and the catalytic efficiency measured as $^{app}k_{cat}/^{app}K_M$ (Figure 3B). Au₁₀Pt₄₂ or Cu₂Pt₃₉ bmNCs grown in the C_{6His} coordination module rendered similar number of Pt atoms (42 vs 39 atoms of Pt with a relative abundance of Pt⁰ of 22.9% and 22.81%, for Au₁₀Pt₄₂@C_{6His} and Cu₂Pt₃₉@C_{6His}, respectively) and thus, catalytic efficiencies (3119 vs 2353 for Au₁₀Pt₄₂@C_{6His} and Cu₂Pt₃₉@C_{6His}, respectively). However, the insertion of Pt atoms does not seem to be the only parameter that encodes the catalytic performance of the nanozymes, but rather has a multi-

factorial origin. In a clear example, Au₇Pt₅₀@C_{6His} outperformed Au₅Pt₅₇@C_{6Cys} 2-fold in terms of peroxidase-like activity with similar number of Pt atoms. The oxidation state of the metals also plays a role in the catalytic activity, being the hybrids with higher content of Pt⁰ the most active in peroxidation reactions, in accordance with previous reports.^[59,63] Additionally, the synergy between oxidation states of the same metal needs to be considered. In this sense, the coexistence of Pt⁰ and Pt^{II} oxidation states in the hybrids enhanced catalysis, as has been previously observed for other systems.^[56,64] This premise is observed in our top-performing nanozymes, i.e., Au₁₀Pt₄₂@C_{6His} and Au₇Pt₇₆@C_{6Cys}, which display similar Pt⁰:Pt^{II} stoichiometry (20/25:63/66) and catalytic turnovers (Figure 3A; and Table S7, Supporting Information).

Deeper investigations were performed to elucidate the composition-activity relationship of the hybrids. The measurement of $^{app}K_M$ for the library nanozymes revealed interesting

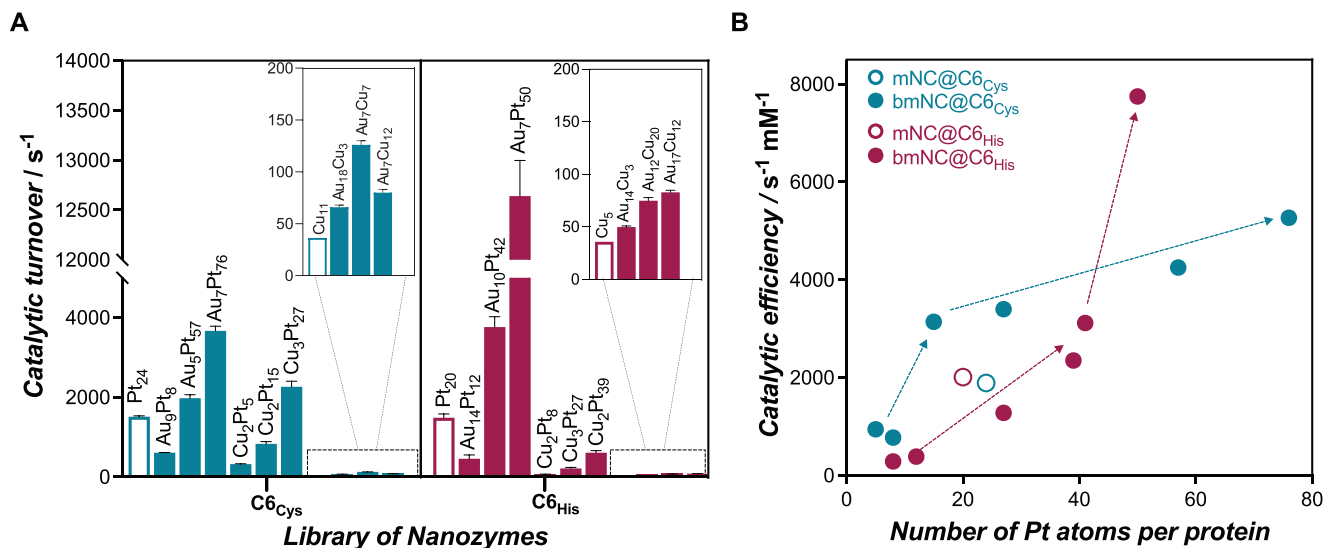


Figure 3. Characterization of the peroxidase-like activity of the nanozymes. A) Catalytic turnovers measured for the whole family of nanozymes built in this work. B) Evolution of the catalytic efficiency ($^{app}k_{cat}/^{app}K_M$) of the nanozymes according to their Pt content.

results when using PG as substrate (Table S7, Supporting Information). While Au_xPt_y family rendered similar or even higher $^{app}K_M$ than that measured for the natural HRP — from 0.47 ± 0.05 to 1.63 ± 0.22 mM versus 0.67 ± 0.03 mM for the hybrids and HRP, respectively — the affinity toward the substrate was markedly increased in Cu-loaded nanozymes, with measured values as low as 0.14 ± 0.03 mM for $Au_{14}Cu_3@C6_{His}$. Such low $^{app}K_M$ was only achieved with the smaller hybrids of the library, most of them within the Au_xCu_y formulation. Interestingly, these values are lower than those reported for other Au/Pt NPs with peroxidase-like activity (K_M of 651 mM for pyrogallol),^[65] and are within the range of values reported for hemin-loaded nanozymes (K_M from 0.4 to 1.2 mM),^[66,67] and the natural HRP enzyme (K_M of ca. 0.8 mM).^[68]

When studying the effect of the coordinating modules on the catalytic parameters, the maximum velocity (V_{max}) measured for Cys-variants was limited to 11 s⁻¹, regardless of the size of the NCs. Hence, the maximum substrate saturation was maintained nearly constant and independent of the size of the NCs (Figure 4A). This value slightly improved that obtained for monometallic Pt@C6_{Cys} ($V_{max} = 8.92 \pm 0.29$ μmol min⁻¹). On the other hand, His module permitted the evolution toward higher catalytic velocities, with a maximum of 37.90 ± 1.07 μmol min⁻¹. This effect highlights the influence of the protein backbone on the catalytic performance of the nanozyme, and might be related to the different accommodation, orientation, and stabilization of the NCs provided by the two protein modules.

2.3.2. Mechanism of Peroxidation

Although these hybrids could be characterized following enzyme-like kinetics, the mechanism of the mNCs has not been yet revealed. For this purpose, we studied the role of different reactive species in the oxidation of pyrogallol mediated by the engineered hybrid biocatalysts. For that, we studied the peroxi-

dation reaction of $Au_7Pt_{50}@C6_{His}$ nanozyme in presence of assorted scavengers of reported reactive species that are usually involved in peroxidation reactions. Thus, 2-propanol to remove hydroxyl radicals, sodium azide (NaN_3) for singlet oxygen, triethylamine (TEA) as metal blocker, and L-ascorbic acid (L-AA) as superoxide anion scavenger were added separately and the activity under those conditions was measured (Figure S16, Supporting Information). As depicted in Figure 4B, both TEA and L-AA depleted completely the peroxidase-like activity of the clusters, revealing that superoxide anions and metal blockers play a major role in substrate oxidation. Also, a partial reduction of the activity was observed when NaN_3 was added to the reaction, which suggests that singlet oxygen species are also present in the peroxidation event. Interestingly, we demonstrated that hydroxyl radicals ($\cdot OH$) are not involved in the mechanism of pyrogallol peroxidation. The absence of $\cdot OH$ radicals in the mechanism is highlighted as one of the main differences with natural peroxidases (Figure S17 and Table S8, Supporting Information), and has been suggested for similar nanozymes, such as the Fe-single atoms nanozymes reported by Wu et al.^[69]

2.3.3. Catalytic Stability of the Nanozymes

This work aims to build catalytic biomaterials for long-term use. As mentioned above, while the deployment of metal NCs is highly attractive due to their functionality, the tendency to aggregate in solution restricts their application. In this respect, the protein-templated synthesis can enhance the NC stability and overcome the formation of aggregates. However, the preferential utilization of NCs, rather than natural enzymes, will be determined by the robustness of the NCs upon long-term storage and under biologically relevant conditions. Thus, we studied the stability of the hybrids over time, pH and temperature ranges, and under high peroxide concentrations.

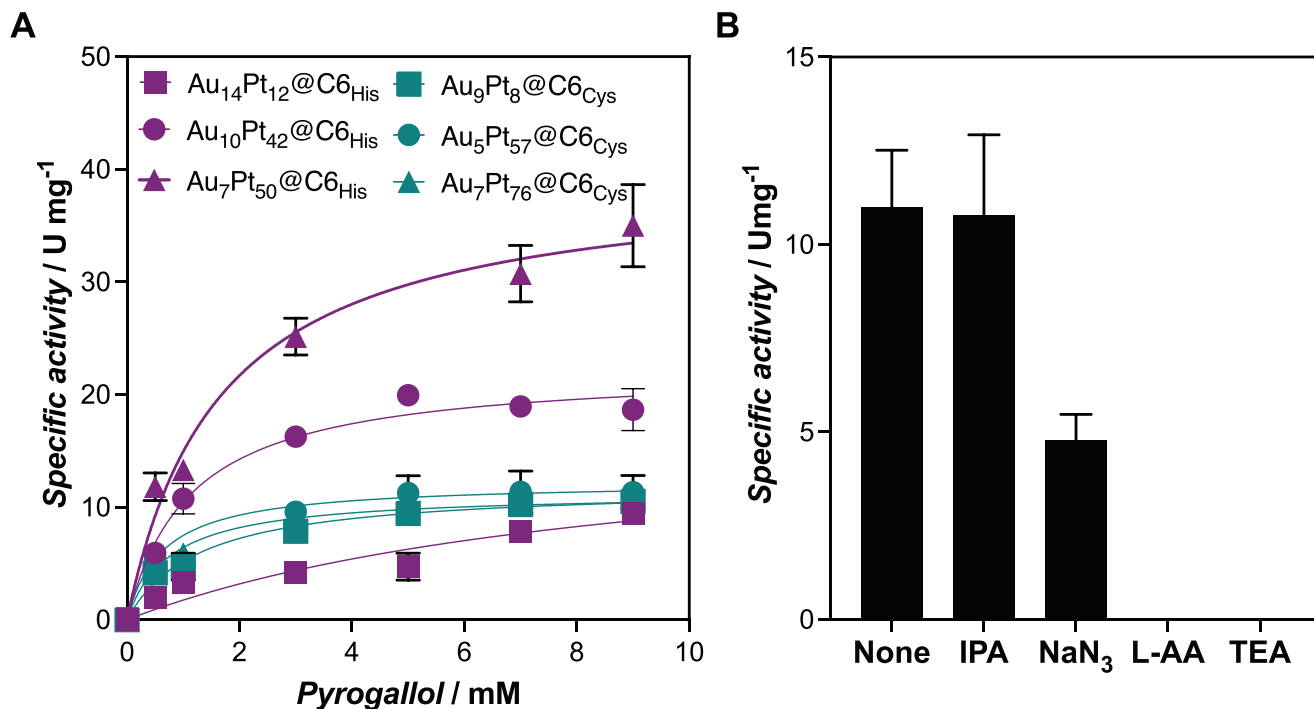


Figure 4. Catalytic study of the nanozymes. A) Michaelis-Menten curves measured for the peroxidation of PG by Au_xPt_y@ nanozymes. B) Specific activity, as U mg⁻¹, measured for Au₇Pt₅₀@C6_{His} in presence of assorted scavengers for reactive species (IPA, sodium azide, L-AA and TEA).

First, the robustness of the catalytic materials upon long-term storage at 4 °C was measured. For that, the specific activity of the nanozymes, both mNC and bmNC, was tracked up to 60 days. As observed in **Figure 5A**, we detected a slight drop in the peroxidase-like activity over time for some of the formulations. While smallest nanoclusters maintained their activity during the assayed timeframe, Au₇Pt₅₀@C6_{His} nanozyme experienced a marked activity drop of 40% upon 60 days storage at 4 °C. It is worth noting that non-protected nanoclusters, i.e., naked-nanoclusters, experience a decline in their catalytic performance within a few days (Figure S7, Supporting Information). In addition, other protein-protected nanozymes in which the nanomaterial remains exposed on the surface of the biomacromolecule have reported limited shelf-stability, e.g. bimetallic NCs stabilized by antibodies, which lost their activity after only 10 days.^[19]

For the following experiments, we focused on the characterization of the top-performing catalytic nanozyme, Au₇Pt₅₀@C6_{His}, as a potential hybrid material that could overcome the robustness issues associated with HRP enzyme. As depicted in **Figure 5B**, the highest catalytic activity of the hybrid was attained at pH 7, with significant activity displayed at pH 6 and 8 (higher than 75% of the maximum activity is conserved). Higher pH values were not tested due to the auto-oxidation of PG substrate at basic pH. Both the natural peroxidases and most of the recently discovered peroxidase nanozymes perform catalysis under acidic environments, with an optimum pH for HRP between 5–6, which limits their usage in numerous biosensing, biomedical, and pharmaceutical applications.^[70] Satisfactorily, the nanozyme shows a broad pH operational window, with less than 25% loss of activity at pH 8.0. Moreover, the ability of Au₇Pt₅₀@C6_{His} to keep its catalytic performance after incubation at high temperatures, i.e.,

60 °C, was demonstrated (Figure 5C). Remarkably, the nanozyme retained its activity — showing less than 8% of activity loss — while the mimicked enzyme, i.e., HRP, was significantly damaged, showing no-activity upon being incubated for 20 min at 60 °C.

One of the difficulties encountered in the use of natural peroxidases in technological and industrial applications is related to their low stability under high hydrogen peroxide concentrations. Most of the nanozymes reported require high hydrogen peroxide concentrations, i.e., over 100 mM,^[71] to carry out the peroxidation reaction. Only few of them, such as Mn/Au hybrids and Au/Ag nanostructures with 0.6 and 1.1 μm, respectively,^[72,73] have shown similar low H₂O₂ detection limits to the nanozymes reported herein. Our Au₇Pt₅₀@C6_{His} nanozyme is tolerant to hydrogen peroxide concentrations to which natural enzymes are poisoned and remain inactive, with only a 25% reduction in its activity observed at 500 mM of peroxide. Moreover, the nanozyme can operate at hydrogen peroxide concentrations as low as 0.01 mM (Figure 5D).^[71,74] Therefore, the high stability and robustness denoted by the nanozymes enable the use of this hybrid catalytic material for technological applications in which high hydrogen peroxide concentrations are demanded.

2.4. Fabrication of Films of Nanozymes

Finally, we have approached the first reported top-down strategy to deposit NCs on surfaces. The benefits of NC-loaded biofilms are not only relevant for the fabrication of reusable catalytic materials, but also for the protection of the nanomaterial, which remains embedded into a solid structure. These biomaterials can

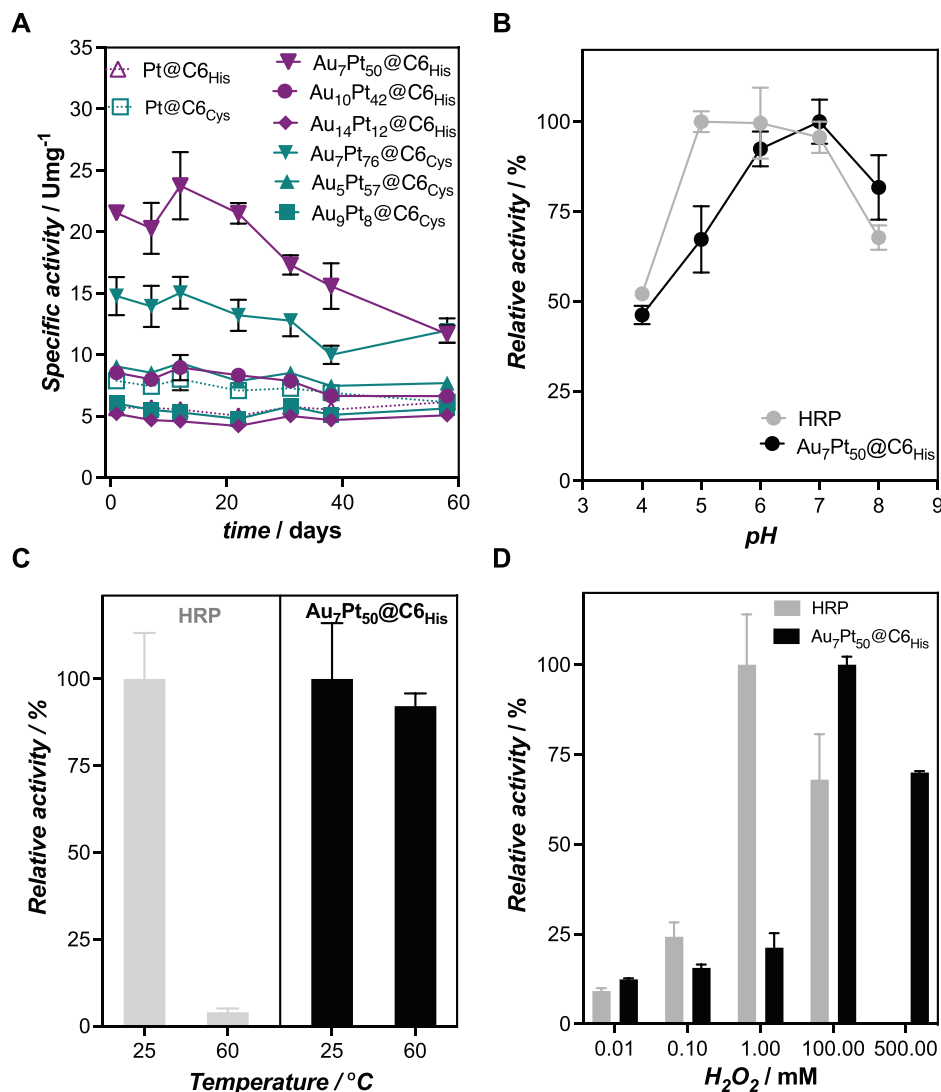


Figure 5. Assessment of the robustness of the peroxidase-like activity of the nanozymes. A) Shelf-stability measured for Au_xPt_y and Pt nanozymes for 60 days. B) pH activity profile of Au₇Pt₅₀@C6_{His} nanozyme and HRP enzyme. C) Measured relative activity of Au₇Pt₅₀@C6_{His} nanozyme and HRP enzyme upon incubation at 25 and 60 °C. D) Measured relative activity of Au₇Pt₅₀@C6_{His} nanozyme and HRP enzyme at increasing hydrogen peroxide concentrations (from 0.01 to 500 mM).

be assembled guided by the self-assembly capabilities of CTPR proteins, which form nanostructured ordered films.^[75,76] Herein, we aim to harness the assembling driving force of CTPR proteins to arrange the Au₇Pt₅₀@C6_{His} hybrid into self-standing catalytic films. For that, a 3% (w/v) solution of Au₇Pt₅₀@C6_{His} was deposited on the surface of a hydrophobic Teflon tape (Figure 6A, inset picture), which resulted in continuous self-standing protein films, similar to the ones obtained for non-functionalized CTPR proteins. As the assembly of the film is governed by weak interactions, which are non-stable in water, the film was chemically cross-linked with 1% of glutaraldehyde (GA) for 24 h (details of the synthesis in the Supporting Information).^[39,40] Importantly, the GA cross-links the protein scaffold to preserve the integrity of the film in water but leaves the NCs unmodified. The film could be manipulated and used in catalytic reactions in aqueous medium (Figure S18, Supporting Information). A

Scanning Electron Microscopy (SEM) observation of the surface of the film rendered a full-covered grainy topology (Figure 6A). An insightful characterization of the film by Scanning Transmission Electron Microscopy (STEM) revealed the presence of well-dispersed, homogeneous nanoclusters of ≈2 nm with high crystalline lattices. Additionally, the Energy Dispersive Spectroscopy (EDS) spectrum of a single nanozyme confirmed the coexistence of Pt and Au within the same particle (Figure 6B; and Figures S19 and S20, Supporting Information).

In order to measure the catalytic activity of the films, thinner films that diminish diffusion issues and remain glued to the surface of a multiwell plate were prepared.^[44] For that, a range of nanozyme concentrations from 20 to 282 μM was tested, resulting optimal the deposition of 5 μL at 100 μm. Hence, we achieved thin films that were tightly adhered to the bottom of the 96-well plate, minimizing thereby the interference in the catalytic

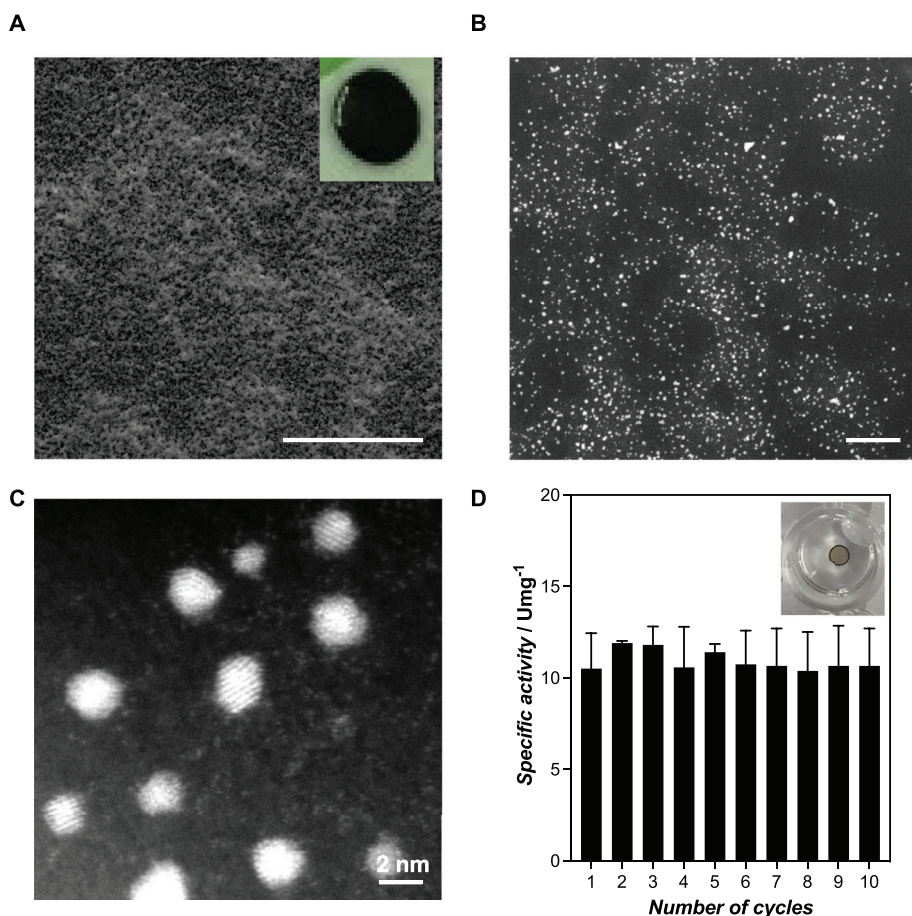


Figure 6. Structural and catalytic characterization of nanozyme films. A) SEM pictograph of nanozyme films synthesized by the self-assembly of 300 μl of a 3.1 mg ml^{-1} solution of $\text{Au}_7\text{Pt}_{50}@C6_{\text{His}}$ (inset: picture of the film) (scale bar: 30 μm). B) STEM pictograph of the nanoclusters arranged into a thin film produced by $\text{Au}_7\text{Pt}_{50}@C6_{\text{His}}$ (scale bar: 30 μm). C) Zoomed in detail of the STEM image in B) in which the crystalline lattices of the NCs are observed (scale bar: 2 nm). D) Recovered specific activity of the films in 10 consecutive peroxidation reactions (inset: thin film deposited on the surface of the well of a 96-well plate).

measurements by UV–vis (Figure S21, Supporting Information). Fabricated films showed high reproducibility, with a measured deviation of the catalytic performance of 11.2% (Figure S22, Supporting Information). To verify the reusability of the nanozyme films, 10 consecutive catalytic cycles were carried out on the same film. After each catalytic cycle, the films were washed 3 times with water prior to the following cycle (details in Supporting Information). The average specific peroxidase-like activity of the nanozyme films was $10.92 \pm 1.23 \text{ U mg}^{-1}$, and was nearly unaltered during the experiment (Figure 6D). Compared to the specific activity in solution — $19.14 \pm 1.31 \text{ U mg}^{-1}$ —, the arrangement of the nanozymes into films showed a foreseeable drop in the activity of 57%, most likely due to diffusion issues. A similar effect was reported before for the embedment of enzymes into protein films.^[39]

3. Conclusion

Nanozymes have recently emerged as artificial biocatalysts with excellent catalytic properties that aim to replace natural enzymes by overcoming their limitations. However, to embrace a

wide number of applications, it is crucial to develop novel approaches to achieve tunable, highly catalytic, stable, and reusable nanozymes. This study introduces an innovative nanozyme fabrication methodology that relies on the in situ growth and stabilization of monometallic and bimetallic nanoclusters within engineered protein scaffolds. The selection of the CTPR scaffold, a robust, superstable, and highly-engineerable module, ensures the structural integrity of the protein template during modification and nanocluster synthesis. The modularity and versatility of the CTPR protein make this scaffold particularly attractive for the stabilization of nanoclusters, compared to natural protein sequences, which are less robust and less easily engineered. The introduction of a set of either histidine or cysteine residues oriented within the inner cavity of the protein, from which the NCs are tethered, protects the resulting nanomaterials. On the other hand, the synthesis of bimetallic nanoclusters expands the catalytic profile of the engineered nanozymes. Importantly, bimetallic nanoclusters showed, among other activities, a peroxidase-like kinetics that fitted a Michaelis-Menten model, confirming the development of a new class of nanozymes. Further investigation that considered the nature of the protein scaffold (composed by

either Cys or His metal-coordination modules), the metal composition of the bmNCs, the size of the bmNCs, and the catalytic activity of the nanozymes, revealed the bimetallic nanozymes with highest Pt content, as the best peroxidase-like catalysts. However, the catalytic activity of nanozymes is influenced by factors other than Pt load. The oxidation state of the metals and the nature of the binding module used for the accommodation of the nanoclusters also have a significant impact on the catalytic performance of the nanozymes. Additionally, the coexistence of Pt^{II}/Pt⁰ may play a role in the performance of the hybrids enhancing the peroxidative performance. Furthermore, for CTPR system, the best results were achieved using His ligands with a relatively high contribution from Pt⁰. The precise allocation of the mNCs on the protein scaffold has resulted in nanozymes with high colloidal stability and enhanced catalytic performance, as well as improved long-term catalytic stability.

Unlike natural enzymes that become specialists in catalyzing specific reactions, nanozymes reach a palette of chemical redox reactions, as demonstrated here with the reported peroxidase, oxidase, catalase, and superoxide dismutase-like activities. Moreover, these hybrid materials are significantly more stable than natural peroxidases and less prone to inactivation by pH or temperature. This fact raises the herein presented nanozymes as outstanding candidates to replace enzymes in numerous technological applications. Finally, and due to the virtue of CTPR proteins to self-assemble into solid materials, a strategy for the top-down deposition of nanoclusters is presented. We achieved stable, efficient, and reusable solid catalytic materials. In conclusion, this comprehensive study on the interplay between the composition and the activity of the nanozymes has provided a solid strategy for the development of à-la-carte nanozymes with high stability and robustness.

4. Experimental Section

Design of CTPR Modules: The consensus tetratricopeptide repeats (CTPR) proteins were previously engineered to introduce strategic metal-coordinating sites based on a tetra-histidine (His) or a tetra-cysteine (Cys) per CTPR motif.^[32] Two different proteins (His and Cys-based) with six CTPR (C6) modules were fabricated by combining these mutated CTPR motif. Thus, these engineered proteins include 16 coordinating residues and proteins are defined as C6-His and C6-Cys. In C6_{Cys} proteins, the coordinating residues were introduced at the positions 2, 6, 9, and 13 of the CTPR motif. Meanwhile, in the C6_{His}, the coordinating residues were introduced at following positions 2, 5, 6, and 9 of the CTPR motif. To improve the solubility in aqueous media, the engineered CTPR proteins have an additional C-terminal solvating helix with polar residues.

Expression and Purification of CTPR Protein: Synthetic gene for the desired proteins (C6-Cys and C6-His) in pProEx-HTA vector, coding for N-terminal hexa-histidine tag and ampicillin resistance, was expressed in *Escherichia coli* C41 (DE3) after induction with 1 mM isopropyl β-D-thiogalactoside (IPTG) at an optical density of 0.6–0.8 followed by 18 h growth at 20 °C. The cell pellets were suspended in lysis buffer (500 mM sodium chloride, 500 mM urea, 50 mM Tris-HCl pH 8.0) and lysed by sonication. After that, the pellet was frozen at –20 °C at least for one day. The proteins (C6-Cys and C6-His) were purified from the supernatant using standard Ni-NTA affinity purification protocol. The N-terminal hexa-histidine tag was then cleaved from the CTPR proteins using the Tobacco Etch Virus (TEV) protease. As a final step, the aqueous solutions of CTPRs were dialyzed against 10 mM phosphate buffer pH 7.4 at 4 °C using a dialysis membrane with molecular weight cutoff of 10 kDa. Protein con-

centration was estimated by UV–vis at 280 nm, using the molar extinction coefficients calculated from the amino acid composition.

Synthesis and Purification of the Nanozymes: An adapted synthesis method^[31] was used for the synthesis of protein-templated metal NCs. Dithiothreitol (DTT, final concentration of 1 mM) was mixed with the C6-Cys scaffold (30 min incubation at 0 °C) to reduce the protein disulfide bonds and to allow the nanoclusters formation near the coordinating-metal residues. First, the protein samples in phosphate buffered saline (50 mM of PB and 150 mM of NaCl at pH 7.0) were changed to pH 10 using PD 10 desalting columns. Second, the proteins (1 mL at 20 μM in phosphate buffered saline at pH 10) were incubated with the corresponding metal salts to allow the coordination with the Cys and His residues (list of used equivalents collected in Table S1, Supporting Information). The used metal salts were chloroauric acid (HAuCl₄), potassium tetrachloroplatinate (K₂PtCl₄), and copper sulfate (CuSO₄). Mixtures were incubated for 30 min to allow the binding of the metal ions to the metal-coordinating sites. After this first incubation, the reduction of the metal salts was achieved with sodium L-ascorbate (SA). The samples were heated up to 50 °C and stirred to 800 rpm. The reducing agent was added according to the metal concentration of each reaction in a molar excess of 100. The mixture was incubated for 72 h. The protein metal NCs were centrifuged (1 h, 4 °C, 15 000 rpm) to remove formed nanoparticles. The supernatant was taken after centrifugation and concentrated up to 500 μL using Amicon filters *cut-off* 10 kDa and purified by PD 10 desalting columns. Protein concentration was estimated by BCA assays by dilutions of the protein metal NCs.

Supporting Information

Supporting Information is available from the Wiley Online Library or from the author.

Acknowledgements

The authors thank Gabriela Guedes, Andoni Rodriguez, and Alessandro Silvestri for their inestimable help in the characterization of the nanozymes. The authors thank Dr. D. di Silvio at CIC biomaGUNE for support with the acquisition and analysis of XPS data. A.L.C. acknowledges support by the Agencia Estatal de Investigación Grants: PID2019-111649RB-I00 funded by MCIN/AEI/ 10.13039/501100011033 and Grant PDC2021-120957-I00 funded by MCIN/AEI/ 10.13039/501100011033 and by the “European Union NextGenerationEU/PRTR”. A.L.C. acknowledges support by the European Research Council Grants: ERC-CoG-648071-ProNANO and ERC-PoC-841063- NIMM. This work was performed under the Maria de Maeztu Units of Excellence Program from Q5 the Spanish State Research Agency grant no. MDM-2017-0720. A.B. gratefully acknowledges the financial support from the Spanish Research Agency (AEI) for the financial support (PID2019-110239RB-I00 funded by MCIN/AEI/10.13039/501100011033/ and by the “European Union NextGenerationEU/PRTR”; RYC2018-025923-I from RyC program – MCIN/AEI/10.13039/501100011033 and FSE “invierte en tu futuro”), BBVA Foundation – IN[21]_CBB_QUI_0086, and UPV/EHU- GIU21-033).

Conflict of Interest

The authors declare no conflict of interest.

Data Availability Statement

The data that support the findings of this study are available from the corresponding author upon reasonable request.

Keywords

artificial enzymes, enzyme-like materials, nanoclusters, nanozymes, protein engineering, protein-nanomaterial hybrids, repeat proteins

Received: January 31, 2023
Revised: May 15, 2023
Published online: May 26, 2023

- [1] H. Wang, K. Wan, X. Shi, *Adv. Mater.* **2019**, *31*, 1805368.
- [2] R. Zhang, X. Yan, K. Fan, *Acc. Mater. Res.* **2021**, *2*, 534.
- [3] M. Liang, K. Fan, Y. Pan, H. Jiang, F. Wang, D. Yang, D. Lu, J. Feng, J. Zhao, L. Yang, X. Yan, *Anal. Chem.* **2013**, *85*, 308.
- [4] A. Robert, B. Meunier, *ACS Nano* **2022**, *16*, 6956.
- [5] M. Liang, X. Yan, *Acc. Chem. Res.* **2019**, *52*, 2190.
- [6] A. Asati, C. Kaftanis, S. Santra, J. M. Perez, *Anal. Chem.* **2011**, *83*, 2547.
- [7] S. Wu, R. Snajdrova, J. C. Moore, K. Baldenius, U. T. Bornscheuer, *Angew. Chem., Int. Ed.* **2021**, *60*, 88.
- [8] W.-C. Hu, M. R. Younis, Y. Zhou, C. Wang, X.-H. Xia, *Small* **2020**, *16*, 2000553.
- [9] X. Liu, Z. Liu, K. Dong, S. Wu, Y. Sang, T. Cui, Y. Zhou, J. Ren, X. Qu, *Biomaterials* **2020**, *258*, 120263.
- [10] N. Wang, Q. Sun, J. Yu, *Adv. Mater.* **2019**, *31*, 1803966.
- [11] B. Corain, G. Schmid, N. Toshima, *Metal Nanoclusters in Catalysis and Materials Science: The Issue of Size Control*, Elsevier, Amsterdam **2011**.
- [12] J. P. Wilcoxon, B. L. Abrams, *Chem. Soc. Rev.* **2006**, *35*, 1162.
- [13] Y. Lu, W. Chen, *Chem. Soc. Rev.* **2012**, *41*, 3594.
- [14] L. Shang, S. Dong, G. U. Nienhaus, *Nano Today* **2011**, *6*, 401.
- [15] C.-J. Yu, T.-H. Chen, J.-Y. Jiang, W.-L. Tseng, *Nanoscale* **2014**, *6*, 9618.
- [16] X. Meng, I. Zare, X. Yan, K. Fan, *Wiley Interdiscip. Rev.: Nanomed. Nanobiotechnol.* **2020**, *12*, 1602.
- [17] T. Chen, H. Lin, Y. Cao, Q. Yao, J. Xie, *Adv. Mater.* **2022**, *34*, 2103918.
- [18] A. Yao, Y. Du, M. Han, Y. Wang, J. Hu, Q. Zhu, H. Sheng, M. Zhu, *Nano Res.* **2023**, *16*, 1527.
- [19] V. Mora-Sanz, L. Saa, N. Briz, V. Pavlov, *Chem. Mater.* **2020**, *32*, 8286.
- [20] Y.-W. Lin, *Molecules* **2019**, *24*, 2743.
- [21] J. Fischer, D. Renn, F. QUITTERER, A. Radhakrishnan, M. Liu, A. Makki, S. Ghorpade, M. Rueping, S. T. Arold, M. Groll, J. Eppinger, *ACS Catal.* **2019**, *9*, 11371.
- [22] C. M. Thomas, T. R. Ward, *Chem. Soc. Rev.* **2005**, *34*, 337.
- [23] U. Markel, D. F. Sauer, J. Schiffels, J. Okuda, U. Schwaneberg, *Angew. Chem., Int. Ed.* **2019**, *58*, 4454.
- [24] H.-S. Park, S.-H. Nam, J. K. Lee, C. N. Yoon, B. Mannervik, S. J. Benkovic, H.-S. Kim, *Science* **2006**, *311*, 535.
- [25] E. Meggers, *Chem. Commun.* **2009**, *9*, 1001.
- [26] K. Okrasa, R. J. Kazlauskas, *Chemistry* **2006**, *12*, 1587.
- [27] J. Xie, Y. Zheng, J. Y. Ying, *J. Am. Chem. Soc.* **2009**, *131*, 888.
- [28] T. Zhou, Y. Huang, W. Li, Z. Cai, F. Luo, C. J. Yang, X. Chen, *Nanoscale* **2012**, *4*, 5312.
- [29] S. Kanbak-Aksu, M. N. Hasan, W. R. Hagen, F. Hollmann, D. Sordi, R. A. Sheldon, I. W. C. E. Arends, *Chem. Commun.* **2012**, *48*, 5745.
- [30] P. Maity, S. Xie, M. Yamauchi, T. Tsukuda, *Nanoscale* **2012**, *4*, 4027.
- [31] A. Aires, I. Llarena, M. Moller, J. Castro-Smirnov, J. Cabanillas-Gonzalez, A. L. Cortajarena, *Angew. Chem., Int. Ed.* **2019**, *58*, 6214.
- [32] A. Aires, V. Fernández-Luna, J. Fernández-Cestau, R. D. Costa, A. L. Cortajarena, *Nano Lett.* **2020**, *20*, 2710.
- [33] C. Bernal, K. Rodríguez, R. Martínez, *Biotechnol. Adv.* **2018**, *36*, 1470.
- [34] L. Huang, D.-W. Sun, H. Pu, C. Zhang, D. Zhang, *Food Hydrocolloids* **2023**, *135*, 108138.
- [35] B. Jiang, D. Duan, L. Gao, M. Zhou, K. Fan, Y. Tang, J. Xi, Y. Bi, Z. Tong, G. F. Gao, N. Xie, A. Tang, G. Nie, M. Liang, X. Yan, *Nat. Protoc.* **2018**, *13*, 1506.
- [36] G. Mechrez, M. A. Krepker, Y. Harel, J.-P. Lellouche, E. Segal, *J. Mater. Chem. B* **2014**, *2*, 915.
- [37] A. Huang, G. Qin, B. D. Olsen, *ACS Appl. Mater. Interfaces* **2015**, *7*, 14660.
- [38] A. Härtl, E. Schmich, J. A. Garrido, J. Hernando, S. C. R. Catharino, S. Walter, P. Feulner, A. Kromka, D. Steinmüller, M. Stutzmann, *Nat Mater* **2004**, *3*, 736.
- [39] D. Sánchez-deAlcázar, S. Velasco-Lozano, N. Zeballos, F. López-Gallego, A. L. Cortajarena, *ChemBioChem* **2019**, *20*, 1977.
- [40] A. Rodríguez-Abetxuko, D. Sánchez-deAlcázar, A. L. Cortajarena, A. Beloqui, *Adv. Mater. Interfaces* **2019**, *6*, 1900598.
- [41] C. Marquié, *J. Agric. Food Chem.* **2001**, *49*, 4676.
- [42] P. Couleaud, S. Adan-Bermudez, A. Aires, S. H. Mejías, B. Sot, A. Somoza, A. L. Cortajarena, *Biomacromolecules* **2015**, *16*, 3836.
- [43] T. Z. Grove, L. Regan, A. L. Cortajarena, *J. R. Soc., Interface* **2013**, *10*, 20130051.
- [44] D. Sanchez-deAlcazar, D. Romera, J. Castro-Smirnov, A. Sousaraei, S. Casado, A. Espasa, M. C. Morant-Miñana, J. J. Hernandez, I. Rodríguez, R. D. Costa, J. Cabanillas-Gonzalez, R. V. Martinez, A. L. Cortajarena, *Nanoscale Adv.* **2019**, *1*, 3980.
- [45] S. H. Mejias, E. López-Martínez, M. Fernandez, P. Couleaud, A. Martin-Lasanta, D. Romera, A. Sanchez-Iglesias, S. Casado, M. R. Osorio, J. M. Abad, M. T. González, A. L. Cortajarena, *Nanoscale* **2021**, *13*, 6772.
- [46] A. Aires, A. Sousaraei, M. Möller, J. Cabanillas-Gonzalez, A. L. Cortajarena, *Nano Lett.* **2021**, *21*, 9347.
- [47] E. Lopez-Martinez, D. Gianolio, S. Garcia-Orrit, V. Vega-Mayoral, J. Cabanillas-Gonzalez, C. Sanchez-Cano, A. L. Cortajarena, *Adv. Opt. Mater.* **2022**, *10*, 2101332.
- [48] T. J. Magliery, L. Regan, *BMC Bioinformatics* **2005**, *6*, 240.
- [49] N. Singh, K. P. Raul, A. Poulouse, G. Mugesh, V. Venkatesh, *ACS Appl. Bio. Mater.* **2020**, *3*, 7454.
- [50] J. Sha, S. Paul, F. Dumeignil, R. Wojcieszak, *RSC Adv.* **2019**, *9*, 29888.
- [51] J. H. Carter, S. Althahban, E. Nowicka, S. J. Freakley, D. J. Morgan, P. M. Shah, S. Golunski, C. J. Kiely, G. J. Hutchings, *ACS Catal.* **2016**, *6*, 6623.
- [52] M.-L. Cui, J.-M. Liu, X.-X. Wang, L.-P. Lin, L. Jiao, L.-H. Zhang, Z.-Y. Zheng, S.-Q. Lin, *Analyst* **2012**, *137*, 5346.
- [53] T.-K. Chang, T.-M. Cheng, H.-L. Chu, S.-H. Tan, J.-C. Kuo, P.-H. Hsu, C.-Y. Su, H.-M. Chen, C.-M. Lee, T.-R. Kuo, *ACS Sustainable Chem. Eng.* **2019**, *7*, 15479.
- [54] A. Mocanu, I. Cernica, G. Tomoia, L.-D. Bobos, O. Horovitz, M. Tomoia-Cotisel, *Colloids Surf. A* **2009**, *338*, 93.
- [55] L. Casella, M. Gullotti, *J. Inorg. Biochem.* **1983**, *18*, 19.
- [56] N. Wu, L. Jiao, S. Song, X. Wei, X. Cai, J. Huang, M. Sha, W. Gu, W. Song, C. Zhu, *Anal. Chem.* **2021**, *93*, 15982.
- [57] M. Gao, Z. Yang, H. Zhang, J. Ma, Y. Zou, X. Cheng, L. Wu, D. Zhao, Y. Deng, *ACS Cent. Sci.* **2022**, *8*, 1633.
- [58] F. Molaabasi, M. Sarparast, M. Shamsipur, L. Irannejad, A. A. Moosavi-Movahedi, A. Ravandi, B. Hajipour Vedom, R. Ghazfar, *Sci. Rep.* **2018**, *8*, 14507.
- [59] Z. Zheng, W. Xie, M. Li, Y. H. Ng, D.-W. Wang, Y. Dai, B. Huang, R. Amal, *Nano Energy* **2017**, *41*, 233.
- [60] A. Harada, H. Fukushima, K. Shiotsuki, H. Yamaguchi, F. Oka, M. Kamachi, *Inorg. Chem.* **1997**, *36*, 6099.
- [61] M. Takahashi, H. Koizumi, W.-J. Chun, M. Kori, T. Imaoka, K. Yamamoto, *Sci. Adv.* **2017**, *3*, 1700101.
- [62] D. Tongsakul, S. Nishimura, K. Ebitani, *ACS Catal.* **2013**, *3*, 2199.
- [63] L. Hui, Y. Xue, C. Xing, Y. Liu, Y. Du, Y. Fang, H. Yu, C. Zhang, F. He, Y. Li, *Nano Energy* **2022**, *95*, 106984.
- [64] F. C. Meunier, L. Cardenas, H. Kaper, B. Šmíd, M. Vorokhta, R. Grosjean, D. Aubert, K. Dembélé, T. Lunkenbein, *Angew. Chem., Int. Ed.* **2021**, *60*, 3799.
- [65] J.-W. Lee, S. Yoon, Y. M. Lo, H. Wu, S.-Y. Lee, B. Moon, *RSC Adv.* **2015**, *5*, 63757.
- [66] T. Xue, S. Jiang, Y. Qu, Q. Su, R. Cheng, S. Dubin, C.-Y. Chiu, R. Kaner, Y. Huang, X. Duan, *Angew. Chem., Int. Ed.* **2012**, *124*, 3888.

- [67] L. Zhang, F. Ma, J. Lei, J. Liu, H. Ju, *Chem. Sci.* **2017**, *8*, 4833.
- [68] H. Yamaguchi, K. Tsubouchi, K. Kawaguchi, E. Horita, A. Harada, *Chemistry* **2004**, *10*, 6179.
- [69] W. Wu, L. Huang, X. Zhu, J. Chen, D. Chao, M. Li, S. Wu, S. Dong, *Chem. Sci.* **2022**, *13*, 4566.
- [70] Y. He, X. Li, X. Xu, J. Pan, X. Niu, *J. Mater. Chem. B* **2018**, *6*, 5750.
- [71] L. Jiao, W. Xu, H. Yan, Y. Wu, C. Liu, D. Du, Y. Lin, C. Zhu, *Anal. Chem.* **2019**, *91*, 11994.
- [72] I.-H. Yeh, S. Tadepalli, K.-K. Liu, *Sci. Rep.* **2022**, *12*, 19661.
- [73] S. Siddiqui, J. H. Niazi, A. Qureshi, *Mater. Today Chem.* **2021**, *22*, 100560.
- [74] A. P. Nagvenkar, A. Gedanken, *ACS Appl. Mater. Interfaces* **2016**, *8*, 22301.
- [75] A. L. Cortajarena, J. Wang, L. Regan, *FEBS J.* **2010**, *277*, 1058.
- [76] T. Kajander, A. L. Cortajarena, S. Mochrie, L. Regan, *Acta Crystallogr., Sect. D: Biol. Crystallogr.* **2007**, *63*, 800.